Weak acid transport across bilayer lipid membrane in the presence of buffers

Theoretical and experimental pH profiles in the unstirred layers

Yuri N. Antonenko,* Gennady A. Denisov,§ and Peter Pohl‡

*A.N. Belozersky Institute of Physico-Chemical Biology, Moscow State University, Moscow 119899, Russia; §Institute of Mathematical Problems of Biology, Russian Academy of Sciences, Pushchino, Moscow Region, 142292, Russia; ‡Department of Medical Physics and Biophysics, Martin Luther University, O-4010 Halle, Germany

ABSTRACT This paper presents a simple model to describe experimental data on weak acid transport across planar bilayer lipid membrane separating two buffered solutions. The model takes into account multiple proton-transfer reactions occurring in the unstirred layers (ULs) adjacent to the membrane. Differential equations of the model are shown to be reduced to a set of nonlinear algebraic equations. Since the latter equations depend monotonically on unknown variables, they can be easily solved numerically, using bisection method. For the particular system studied experimentally (with acetate as the weak acid and TRIS + MES as the buffer mixture) pH profiles in the ULs are calculated from the model. These results are compared with experimental data obtained using pH microelectrode. The agreement between theoretical and experimental pH profiles is found to be satisfactory. The most pronounced deviations are observed at the UL/bulk solution boundary. To obtain a better correlation between the theoretical and experimental results, two other, less idealized models are considered. They take into account, respectively, (*a*) the electric field arising in the ULs from ion diffusion and (*b*) finiteness of the rates of proton-transfer reactions. However, both acetate membrane fluxes and pH profiles in the ULs computed from these models are found to be close to those of the simple model. One can thus conclude that the difference between experimental and theoretical pH profiles is due to the inconsistency of the generally accepted model of the "unstirred layer", assuming the existence of a strict boundary between the regions of "pure diffusion" and "ideal stirring".

INTRODUCTION

Diffusional ("unstirred") layers (ULs) adjacent to the membrane play an important role in transport of solutes across biological and model bilayer lipid membranes (BLMs) (1–3). In many practically interesting cases, diffusion of solutes through the UL is accompanied by chemical reactions. Among these reactions the dissociation/recombination of the protonated forms of permeants and/or components of the buffer mixture appear to be the most important. Numerous physiologically active weak acids and weak bases like nutrients, metabolites, and drugs can be attributed to these kinds of permeants. Since only the electroneutral forms of these substances are permeable through the membrane, the proton-transfer reactions shift the pH near the membrane from its bulk value. For example, the transfer of weak acid across the membrane will cause a depletion of H^+ in the UL on the *cis* side of the membrane and an enrichment of H^+ in the *trans* UL. This dramatically affects the membrane flux (4, 5). On the other hand, the magnitudes of the pH shifts depend upon the buffer concentration which can control the membrane transport to a considerable extent under some experimental conditions (4, 6). In the present study only homogeneous proton-transfer reactions proceeding in the UL are dealt with; a similar class of processes occurring at the membrane-solution interface (7–10) stays out of our consideration.

In spite of the important role of buffer-involved proton transfer reactions in the transport of substances through membranes the theoretical and experimental studies available (5, 6, 11, 12) seem to be insufficient. Theoretical considerations were made only for two limiting cases, namely, the case of a system containing an excess of buffer and the case where a buffer is absent. For example, Walter and co-workers (6) proposed an algorithm for computing the pH profiles in the absence of buffer. Markin and co-workers (11) derived analytical expressions for pH profiles induced by permeation of amine across BLM in unbuffered solutions. However, in experiments of these authors and in the majority of other works one or other buffer mixtures were used. The model by Antonenko and Yaguzhinsky (12) took into account the buffer, but was valid only in a limiting case of low membrane fluxes. It should finally be noted that in all the previous studies only the membrane flux and the pH shifts near the membrane surfaces were tested experimentally, while theoretical models predicted the distribution of $[H^+]$ and of other solute concentrations in the whole space of UL.

The purpose of the present work is to study a weak acid transport across BLM in the presence of a buffer mixture. In the first part of the work, a particular example of such a system is analyzed in detail, where the weak acid is acetate and the buffer mixture consists of two components. We have calculated the profiles of pH and of other solutes in both UL using a simple model de-

Address correspondence to Dr. Yuri Antonenko, A.N. Belozersky Institute of Physico-Chemical Biology, Moscow State University, Moscow 119899, Russia; FAX, 7-(095)-939-0338, E-mail, libro@genebee.msu.su.

Abbreviations used: UL, unstirred layer; BLM, bilayer lipid membrane; MES, 2-(*N*-Morpholino)ethanesulfonic acid; TRIS, tris(hydroxymethyl)aminomethane; BP, bulk phase.

0006-3495/93/06/1701/10 $2.00

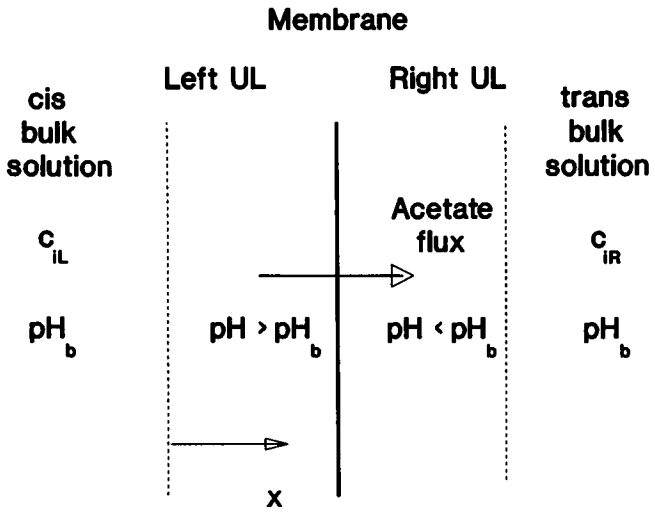

FIGURE 1 Schematic of bilayer lipid membrane with two unstirred layers (*cis* solution contains higher acetate concentration than *trans* solution).

scribed below and two other, more complicated models. By comparing the results calculated from these models we have confirmed the validity of the simplest model for the considered system. Moreover, we suggest a computational method to solve rapidly the equations of the simple model. This method can also be applied to another problem, like the membrane transport of weak bases and carrier-mediated cation/H^+ exchange. In the second part of the work, the calculated pH profiles are compared with the experimental data obtained with the use of a pH microelectrode according to the method suggested earlier (13, 14). These measurements have been carried out on planar BLM as a model membrane system. We find that the theory and experiments agree fairly well. Possible reasons for some quantitative disagreements are discussed.

THEORETICAL

Formulating mathematical models

Let us consider a stationary transport of acetate across bilayer lipid membrane separating two buffer solutions. Both solutions are assumed to be ideally stirred except for the layer of thickness δ adjacent to the membrane surface (Fig. 1). The bulk solutions contain acetate, a mixture of buffers and choline chloride; the acetate concentrations are different while the pH values and the concentrations of all the other solutes are equal on both membrane sides. The flux of protonated acetate across the membrane is determined by

$$\bar{J} = P \cdot ([\mathrm{AceH}]_L - [\mathrm{AceH}]_R), \qquad (1)$$

where P is the permeability and $[\mathrm{AceH}]_L$ and $[\mathrm{AceH}]_R$ are, respectively, the local concentrations of the neutral form of acetate in the immediate vicinity of the left-hand and right-hand surface of the membrane.

Our purpose is to calculate the membrane flux and the profiles of solute concentrations (first of all $[H^+]$) in either UL. We will do this by using three different mathematical models. Each model is the boundary value problem (BVP) for the system of nonlinear differential equations.

In the first model, we make, along with the others, the following two assumptions:

(A.1) The electric field arising from ion diffusion through either UL is negligibly small;

(A.2) The rates of chemical reactions (like dissociation/recombination of water, buffers and acetate) are very high compared to the rate of diffusion through the UL, so that the local chemical equilibrium is maintained.

In the Appendix, we are going to show that these assumptions simplify substantially the numerical algorithm of solving the related BVP by reducing it to a set of algebraic equations linking the quantities $[\mathrm{AceH}]_L$, $[\mathrm{AceH}]_R$, $\bar{J}$ and the local concentrations H_L and H_R of H^+ at the membrane surfaces.

In the second and third model, we reject either A.1 or A.2. This complicates our computations but allows us to test the validity of A.1 and A.2 for the system under consideration by comparing the results calculated from models 2 and 3 with those for model 1.

For the sake of simplicity, we assume that the buffer consists of two components, A = MES and B = TRIS. The experimental buffer mixture contained Mes (weak acid, $pK_A = 6.2$), TRIS (weak base, $pK_B = 8.2$) and β-Alanine (zwitterion, $pK_A = 3.6$, $pK_B = 10.2$). However, if the pH range close to the neutral value pH 7 is dealt with, one can ignore the presence of β-Alanine and take into account MES and TRIS only. Similarly, in the acidic range of pH values one can ignore the presence of TRIS and choose MES = A and β-Alanine = B. Moreover, the general case of a buffer mixture consisting of an arbitrary number of components can be considered in the same way.

Let us first consider the transport of solutes across the left-hand (*cis*) UL. Introduce the coordinate x, $0 \le x \le \delta$, directed from the left-hand boundary of the UL towards the surface of the membrane (Fig. 1). Assume that the transport through the UL is due to the solute diffusion accompanied by the chemical reactions:

$$H^+ + \mathrm{Ace}^- \underset{k_{+1}}{\overset{k_{-1}}{\rightleftarrows}} \mathrm{AceH}; \quad H^+ + OH^- \underset{k_{+2}}{\overset{k_{-2}}{\rightleftarrows}} H_2O; \qquad (2)$$

$$H^+ + \mathrm{Mes}^{2-} \underset{k_{+3}}{\overset{k_{-3}}{\rightleftarrows}} \mathrm{MesH}^-; \quad H^+ + \mathrm{Tris} \underset{k_{+4}}{\overset{k_{-4}}{\rightleftarrows}} \mathrm{TrisH}^+. \qquad (3)$$

In the first and third model, the solute fluxes are described by the Fick diffusion equation, while in the second model the Nernst-Plank approximation is used:

$$J_i = -D_i \, dc_i/dx, \quad i = 1, \ldots, 8 \qquad \text{(first and third model)}; \quad (4)$$

$$J_i = -D_i\,dc_i/dx + D_i(F/RT)c_i z_i E, \quad i = 1, \ldots, 10 \quad \text{(second model)}. \quad (5)$$

Here, J_i, D_i, $c_i(x)$ and z_i, are, respectively, the flux, the diffusion coefficient, the concentration and the valence of the ith species, where 1 = H^+, 2 = Ace^-, 3 = AceH, 4 = OH^-, 5 = A^{2-}, 6 = AH^-, 7 = B, 8 = BH^+, 9 = Cho^+, 10 = Cl^-; F is the Faraday constant, R is the gas constant, T is the absolute temperature and $E(x)$ is the electric field. Note that ions Cho^+ and Cl^- not participating in chemical reactions 2 and 3 are not taken into account in models 1 and 3. Actually these ions do not make any effect on acetate membrane flux provided the electric field effects are neglected.

The mass balance equations are:

$$dJ_i/dx = R_i(c); \quad i = 1, \ldots, 10; \quad c = (c_1, \ldots, c_{10}), \quad (6)$$

where $R_i(c)$ is the specific local rate of expenditure of the ith species in chemical reactions 2 and 3,

$$\begin{aligned} R_1(c) &= R_2(c) + R_4(c) + R_5(c) + R_7(c);\\ R_2(c) &= -R_3(c) = k_{+1}c_3 - k_{-1}c_1c_2;\\ R_4(c) &= k_{+2}[H_2O] - k_{-2}c_1c_4;\\ R_5(c) &= -R_6(c) = k_{+3}c_6 - k_{-3}c_1c_5;\\ R_7(c) &= -R_8(c) = k_{+4}c_8 - k_{-4}c_1c_7;\\ R_9(c) &= R_{10}(c) = 0. \end{aligned} \quad (7)$$

It follows from Eqs. 6 and 7 that:

$$\frac{d}{dx}(J_1 - J_2 - J_4 - J_5 - J_7) = \frac{d}{dx}(J_2 + J_3) = \frac{d}{dx}(J_5 + J_6) = \frac{d}{dx}(J_7 + J_8) = 0, \quad (8)$$

$$\frac{d}{dx}J_9 = 0. \quad (9)$$

The local chemical equilibrium assumption made in the first and second model means that

$$\begin{aligned} &c_1(x)\cdot c_2(x) = K_C\cdot c_3(x); \quad c_1(x)\cdot c_4(x) = K_W;\\ &c_1(x)\cdot c_5(x) = K_A\cdot c_6(x); \quad c_1(x)\cdot c_7(x) = K_B\cdot c_8(x), \end{aligned} \quad (10)$$

where $K_c = k_{+1}/k_{-1}$, $K_W = k_{+2}[H_2O]/k_{-2}$, $K_A = k_{+3}/k_{-3}$ and $K_B = k_{+4}/k_{-4}$ are the equilibrium constants.

Thus, the final system of equations of mass transfer through the left-hand UL is:

(a) for the first model (8 species): 4 equations (10) and 4 equations (8), where the fluxes J_i are expressed in terms of concentrations c_i by (4));

(b) for the second model (10 species): 4 equations (10), the electroneutrality condition

$$\sum_{i=1}^{10} z_i c_i = 0$$

and 5 linearly independent equations (8 and 9), where J_i and $E(x)$ are expressed in terms of c_i by Eq. 5 and

$$E(x) = (RT/F)\cdot\left(\sum_{i=1}^{10} D_i z_i\,dc_i/dx\right)\Big/\left(\sum_{i=1}^{10} D_i z_i^2 c_i\right)$$

(the latter equation results from zero current condition);

(c) for the third model (8 species); 8 first equations (6), where J_i and R_i are expressed in terms of c_i by Eqs. 4 and 7, respectively.

The boundary conditions at $x = 0$ are the known solute concentrations in the *cis* bulk solution,

$$c_i(0) = c_{iL}^0. \quad (11)$$

At $x = \delta$, the fluxes of all species are required to be equal to zero except for J_3 which satisfies Eq. 1, so that

$$J_1 = J_2 = J_4 = \cdots = J_{10} = 0; \quad J_3 = \bar{J}. \quad (12)$$

For the right-hand (*trans*) UL, the equations and the boundary conditions are formulated in the same way.

Method of computation

Numerical algorithm of solving the equations of the first model is described in the Appendix. We have written a FORTRAN program using this algorithm. If requested, this program will be sent to any researcher (a diskette formatted for IBM compatible computer is required). Moreover, we made similar programs to describe the membrane transport of a weak base and the carrier-induced cation/H^+ exchange.

The three-point boundary-value problems corresponding to models 2 and 3 are solved numerically by the Newton finite difference method with the use of the standard computer program DNOKS (15). To do this, the model differential equations are replaced by finite difference equations defined at the uniform mesh with the total number up to 30 points per either UL.

Table 1 lists the parameter values used in our computations. The acetate membrane permeability is available in the literature (16). The diffusion coefficients of H^+, OH^-, CH_3COO^-, and Cl^- are estimated from the Nernst-Einstein equation with the known aqueous limiting ionic conductivities of these ions (17). The diffusivities of the rest solutes are calculated using Wilke-Chang correlation (18) and the known molecular weights of the solutes (M_{Mes} = 195, M_{Tris} = 121, $M_{\beta\text{-Alanine}}$ = 89, $M_{Choline}$ = 105). The kinetic rate constants $k_{\pm1}$, $k_{\pm2}$ are available in the literature (19), but $k_{\pm3}$, $k_{\pm4}$ are not. For this reason the constants $k_{-3,-4}$ are regarded as the varied parameters in this study and $k_{+3,+4}$ are calculated by $k_{+3,+4} = K_{A,B}\cdot k_{-3,-4}$.

Calculated pH profiles

Figs. 2 and 3 show the distribution of pH in the ULs calculated from model 1 at pH 7.5 and 5.0. These and further calculations are carried out for the same conditions as the experimental data available (see Results).

TABLE 1 **List of parameter values used in computations**

Model parameter	Value
P [m · s^{-1}]	$6.9 \cdot 10^{-5}$
δ [m]	$2 \cdot 10^{-4}$
D_1 [m^2 · s^{-1}]	$9.31 \cdot 10^{-9}$
$D_{2,3}$ [m^2 · s^{-1}]	$1.03 \cdot 10^{-9}$
D_4 [m^2 · s^{-1}]	$5.26 \cdot 10^{-9}$
$D_{5,6}$ [m^2 · s^{-1}]	$4.9 \cdot 10^{-10}$
$D_{7,8}$ [m^2 · s^{-1}]	$6.6 \cdot 10^{-10}$
D_9 [m^2 · s^{-1}]	$7.1 \cdot 10^{-10}$
D_{10} [m^2 · s^{-1}]	$2.03 \cdot 10^{-9}$
pK_A	6.2
pK_B	8.2
pK_C	4.75
pK_W	14.0
k_{-1} [m^3 · kmol^{-1} · s^{-1}]	10^6
k_{-2} [m^3 · kmol^{-1} · s^{-1}]	$5.2 \cdot 10^7$
$k_{-3,-4}$ [m^3 · kmol^{-1} · s^{-1}]	$10^6 \div 10^{10}$
pH of the bulk solutions [—]	$5 \div 8$
$c^0_{2L} + c^0_{3L}$ [kmol · m^{-3}]	$10^{-2} \div 10^{-1}$
$c^0_{2R} + c^0_{3R}$ [kmol · m^{-3}]	10^{-3}
$c^0_{5L} + c^0_{6L}$, $c^0_{5R} + c^0_{6R}$ [kmol · m^{-3}]	$10^{-3} \div 10^{-1}$
$c^0_{7L} + c^0_{8L}$, $c^0_{7R} + c^0_{8R}$ [kmol · m^{-3}]	$10^{-3} \div 10^{-1}$
$c^0_{9L} + c^0_{9R}$ [kmol · m^{-3}]	0.1

The pH value 5.0 is close to pK of acetate (4.75), whereas pH 7.5 is rather far from pK. It is seen that at low acetate concentrations (and hence low membrane fluxes) pH profiles are linear whatever the bulk pH. At high acetate concentrations, however, the pH profiles are

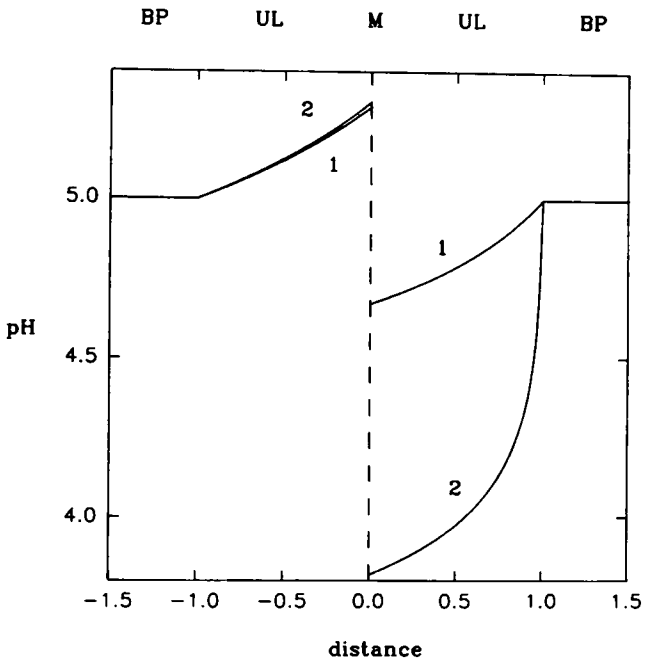

FIGURE 2 The plots of pH versus dimensionless coordinate $y = (x - \delta)/\delta$ calculated from model 1. The bulk pH is 5.0. Acetate concentration at the *cis* side: 1 mM (curve 1), 70 mM (curve 2). Buffer mixture: 1 mM MES and 1 mM TRIS. For other parameters see Table 1. BP, bulk phase; UL, unstirred layer; M, membrane.

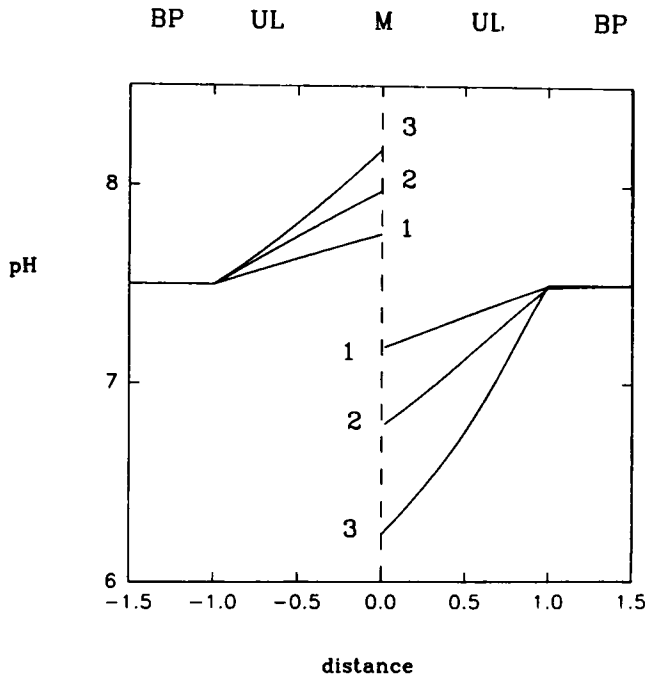

FIGURE 3 The plots of pH versus dimensionless coordinate $y = (x - \delta)/\delta$ calculated from model 1. The bulk pH is 7.5. Acetate concentration at the cis side: 5 mM (curve 1), 20 mM (curve 2), 87 mM (curve 3). Buffer mixture: 1 mM MES and 1 mM TRIS. For other parameters and abbreviations see Table 1 and Fig. 2.

essentially nonlinear especially at the *trans* side with bulk pH 5.0. It is interesting to point out that the increase in the acetate concentration at bulk pH 5.0 does not result in increasing the pH shifts at the *cis* side (Fig. 3). This can be attributed to the increase in the buffer capacity of the solution to which acetate is added.

The profiles shown in (Figs. 2, 3) are calculated for the 1 mM mixture of two buffers with pK 6.2 and 8.2 (MES and TRIS). Figs. 4 and 5 present a series of pH profiles calculated for different concentrations of a 1:1 mixture of two buffers with pK 3.6 (β-alanine) and 6.2 (MES) at bulk pH 5.0 using different concentrations of the weak acid—1 mM (Fig. 4) and 140 mM (Fig. 5). As expected, the pH shifts near the membrane decrease with increasing buffer concentrations. This effect is higher at low acetate concentrations (Fig. 4).

Fig. 6 shows the effect of buffer concentration on the acetate flux at different bulk pH and acetate concentrations. It is seen that at pH 5 the flux does not depend on the buffer capacity (Fig. 5 *A*) while at pH 7.5 and a high acetate concentration the buffer stimulates the membrane flux (Fig. 6 *B*). Different degrees of the effect of buffer at high and low acetate concentrations are in good agreement with a qualitative model proposed in (12), where it was shown that at high acetate concentrations the limiting step of the overall transport switches from membrane to ULs. At pH 5 the total flux is limited by the acetate diffusion through the ULs (16). This process

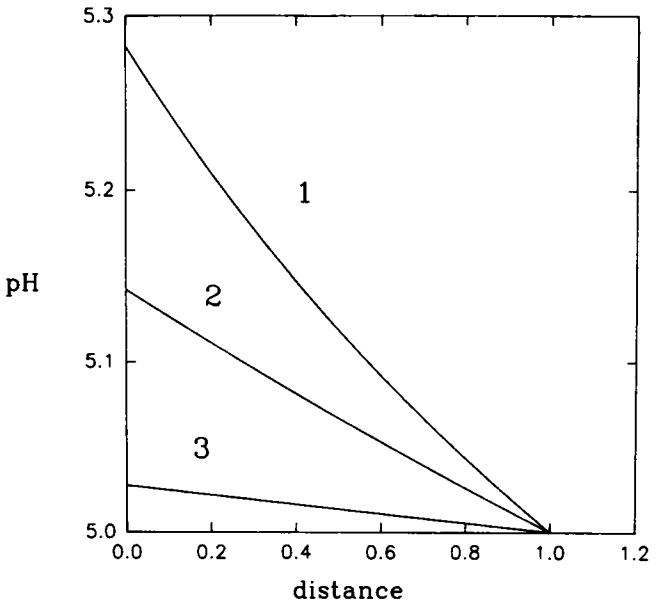

FIGURE 4 The plots of pH versus dimensionless coordinate $y = (x - \delta)/\delta$ calculated from model 1 for the *cis* UL. The bulk pH is 5.0; the acetate concentration at the *cis* side is 1 mM. The concentration of buffer mixture (MES and β-alanine): 1 mM (curve 1), 10 mM (curve 2), 90 mM (curve 3). For other parameters and abbreviations see Table 1 and Fig. 2.

is poorly dependent on the pH distribution in the ULs and hence on the bulk buffer concentration.

Similar calculations from models 2 and 3 are carried out. They show that the electric field arising in the ULs is not high for the system at hand (Fig. 7 *A*) and that the deviations from the local chemical equilibrium can be neglected except for the close vicinity of the membrane surface (Fig. 7 *B, dashed curve*); small deviations from water equilibrium are observed (Fig. 7 *B, solid curve*). The difference in acetate flux calculated in models 2 and 3 with respect to that in model 1 is less than 2 and 5%, respectively. Thus the electric field and deviations from the local chemical equilibrium can be neglected in our model.

EXPERIMENTAL

Materials and methods

BLM is formed on a Teflon partition 1.2 mm in diameter, by a conventional method (20). A membrane-forming solution contains 20 mg phosphatidylcholine from soy beans (Sigma Chemical Co., St. Louis, MO) and 10 mg cholesterol (Merck, Darmstadt, Germany) in 1 ml of *n*-decane. The experiments are carried out at room temperature (21–23°C). Other chemicals from Merck, Darmstadt, Germany.

The measurements of pH shifts near the BLM are carried out by direct method with the help of a pH microelectrode. The system was described in detail in our previous publications (13, 14). It is interesting to point out that basically the same technique was applied independently (21). Briefly, a grass-insulated tip-sensitive antimony pH microelectrode is driven perpendicular to the surface of the BLM through the open space in the rear part of the cell. Typically the electrode tip is ~10 μm. The process of BLM formation and pH microelectrode movements are observed through the transparent window in the front side of the cell. Smooth approach of microelectrode to the membrane is carried out using a hydraulic system attached to the reversible drive. Electric scheme contains a Keithley 617 electrometer connected to a computer through an IEEE interface card. Measurements are performed using ASYST software, results are analyzed using the SIGMAPLOT software package. Voltages are recorded routinely every second with the microelectrode speed 4 μm per second.

Results

Fig. 8 and 9 show experimental pH profiles near BLM induced by different concentrations of acetate added at one side of the membrane. In order to record pH profiles shown in the left-hand sides of Figs. 8 and 9, acetate is added at the same side of the membrane where the pH microelectrode is located, and for the right sides of Figs. 8 and 9, on the opposite side, accordingly. The location of the membrane is determined indirectly from the jump of voltage as described by Antonenko and Bulychev (13). The comparison of Figs. 8 and 9 with theoretical profiles in Figs. 2 and 3 shows that most peculiarities of experimental pH profiles are well described by model 1 of the Theoretical section. The theoretical and experimental values of pH shifts near the membrane correlate well with each other. At pH 5 the pH shift at the *cis* side is practically independent of the acetate concentration while the pH shift at the *trans* side increases substantially with acetate concentration (Fig. 8). At pH 7.5 acetate titrates the pH shifts at both sides of the membrane (Fig. 9). Calculated pH profiles at pH 5.0 (Fig. 8, curve 2 with 70 mM acetate) are convex at the *trans* and concave at

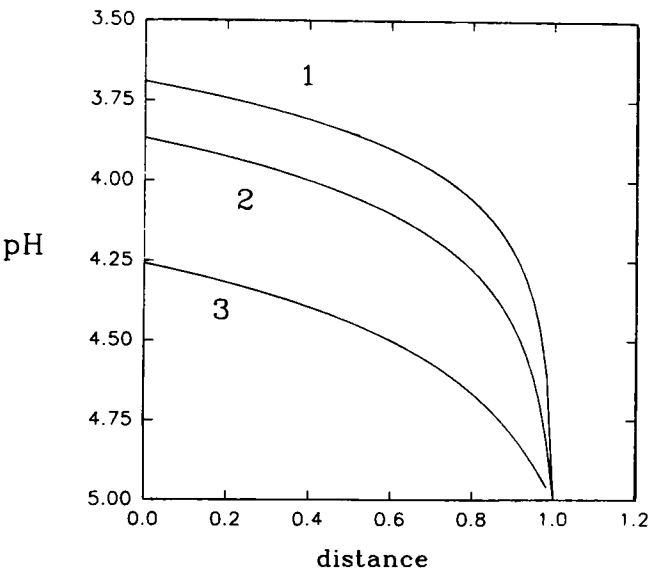

FIGURE 5 The plots of pH versus dimensionless coordinate $y = (x - \delta)/\delta$ calculated from model 1 for the *trans* UL. The bulk pH is 5.0; the acetate concentration at the *cis* side is 140 mM. The concentration of buffer mixture (MES and β-alanine): 1 mM (curve 1), 10 mM (curve 2), 70 mM (curve 3). For other parameters and abbreviations see Table 1 and Fig. 2.

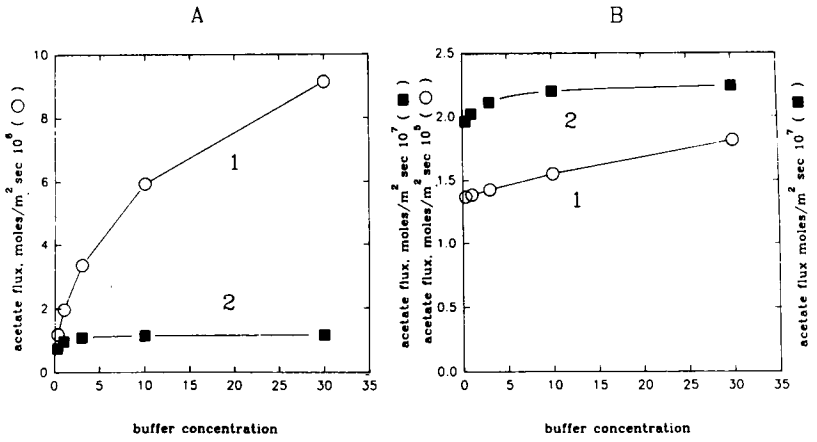

FIGURE 6 The effect of buffer concentration on the acetate membrane flux. (*A*) Acetate concentration in the *cis* solution is 1 mM (curve 1) and 140 mM (curve 2); pH 7.5. (Buffer mixture) 1 mM MES and 1 mM TRIS. (*B*) Acetate concentration is 0.1 mM (curve 1) and 14 mM (curve 2); pH 5.0. Buffer mixture: 1 mM MES and 1 mM β-alanine. For other parameters see Table 1.

the *cis* side. Experimental pH profiles behave the same way. The major qualitative difference of experimental pH profiles from theoretical ones (Figs. 8, 9 and 2, 3) is that the "apparent width of the UL" (which is defined as the width of a zone where the measured pH undergoes its "main" change) depends considerably on the acetate concentration. Theoretical curves do not describe this dependence.

Figs. 10 and 11 show a series of pH profiles recorded at different concentrations of two buffers: MES and β-alanine. It is seen from the comparison of experimental pH profiles (Figs. 10 and 11) with theoretical ones (Figs. 4 and 5) that at the 1 mM acetate concentration (Figs. 4, 10) experimental and theoretical pH profiles correlate well. An increase in the buffer concentration from 1 to 10 mM produces minor effects on the pH shifts, whereas a further increase from 10 to 70 mM reduces pH shifts significantly. At high acetate concentrations the effect of buffers is not so strong (Fig. 11). The variation of the "apparent UL width" is most pronounced at high acetate concentrations (Fig. 11).

Figs. 10 and 11, besides, show the best fit curves derived with the help of the phenomenological equation

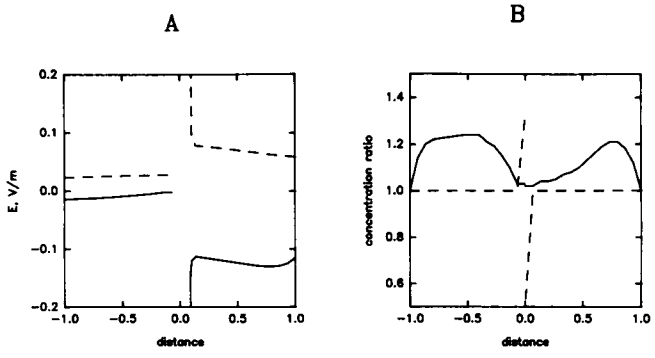

FIGURE 7 The electric field (*A*) and the ratios $r_1 = [Ace^-]\cdot[H^+]/[AceH]/K_c$ and $r_2 = [H^+]\cdot[OH^-]/K_w$ (*B*) in the unstirred layers calculated from model 2 (*A*) and 3 (*B*). (*A: solid curve*) 10 mM acetate at the *cis* side of the membrane and 1 mM at *trans* side, pH 5; (*dashed curve*) 50 mM acetate at the *cis* side and 1 mM at the *trans* side, pH 7.5. B: 100 mM acetate at *cis* side and 1 mM at the *trans* side, pH 7.5. (*Solid curve*) $r_2(x/\delta)$, (*dashed curve*) $r_1(x/\delta)$; $k_{-3,-4} = 10^{10}\ m^3\cdot kmol^{-1}\cdot s^{-1}$, i.e., both the reactions (3) are assumed to be very fast. (*Buffer mixture*) 1 mM MES and 1 mM TRIS. For other parameters see Table 1.

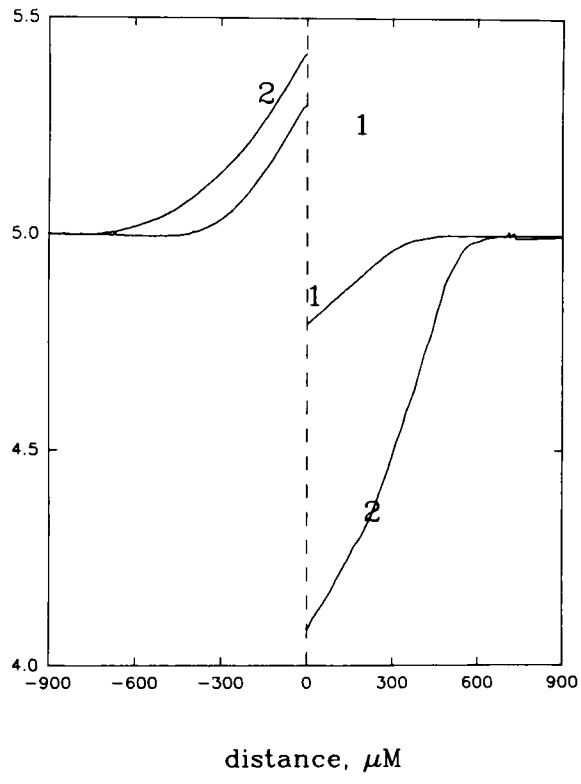

FIGURE 8 Experimental pH profiles near BLM. Acetate concentration at the *cis* side is 1 mM (curve 1) and 70 mM (curve 2). Both the bulk solutions contain 1 mM TRIS, 1 mM MES, 1 mM β-alanine and 100 mM choline chloride; pH 5.0.

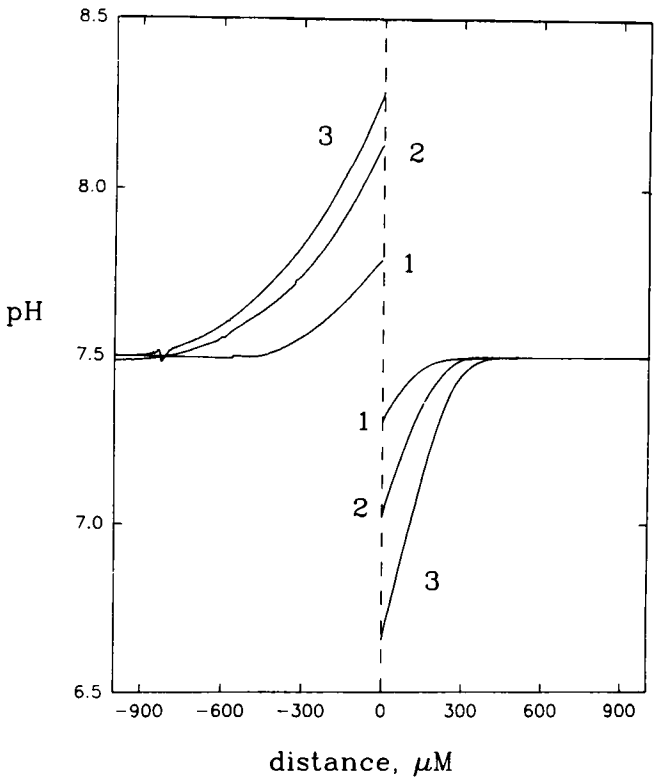

FIGURE 9 Experimental pH profiles near BLM. Acetate concentration at the *cis* side is 5 mM (curve 1), 20 mM (curve 2) and 87 mM (curve 3). Both the bulk solutions contain 1 mM TRIS, 1 mM MES, 1 mM β-alanine and 100 mM choline chloride; pH 7.5. The *cis* solution is unstirred.

$$\mathrm{pH} = \frac{A}{e^{x \cdot k} + B} + \mathrm{pH_b},$$

where x is the distance from the membrane, $\mathrm{pH_b}$ is the bulk pH value and A, B, and k are the fitting parameters. It is obvious that the experimental and best fit curves coincide very well. The parameter $1/k$ has a dimension of distance and gives a rough estimate for the thickness of the unstirred layer. Parameter A describes (roughly) the magnitude of the pH shift, and B measures deviation of the experimental curve from uniexponential curve.

DISCUSSION

It can be seen in the Results section that model 1 describes fairly well the dependence of experimental pH profiles on the concentration of the buffers and acetate. The major deviations between calculated and experimental pH profiles are observed at the UL/bulk solution boundary. The experimental pH curves are smooth in this region and fitted well by exponential, while theoretical profiles undergo a sharp break at the boundary with "complete stirring" zone. These deviations can be exemplified with pH profiles shown in Fig. 9, where "the apparent width of the UL" (see Results) depends strongly on acetate concentration. One can suggest several explanations for these deviations. Let us analyze them in detail.

(*a*) *Strict UL/bulk solution boundary.* The most likely reason for deviations between calculated and measured pH profiles is the inconsistency of the generally accepted model of the UL, where a strict boundary between the regions of diffusion and complete stirring is assumed. If this transition is "smooth", one can expect the existence of a thicker zone where the pH gradually shifts. With this concern we think that further improvement of our model should involve the use of rigorous convective-diffusion equations to describe the distribution of solute concentrations near the membrane as it has already been done in the case of the rotating disk electrode (22) and rotating membrane (23).

(*b*) *Diffusional potential.* Another possible reason for the deviations between theoretical and experimental pH profiles is that in model 1 we neglect the electric field arising from the diffusion of ions with different mobilities. It is known (see for example Denisov et al., 1992) that in some cases these fields can significantly distort

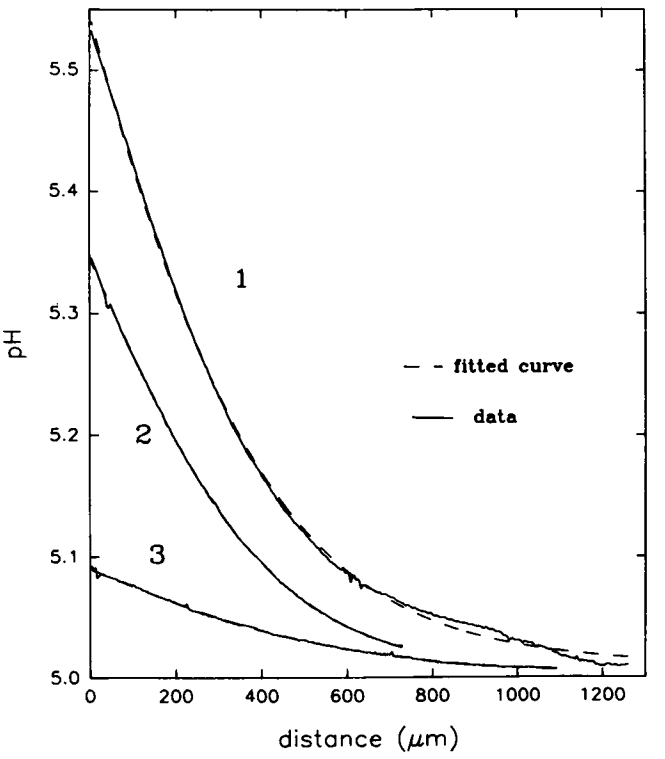

FIGURE 10 Experimental pH profiles measured at the *cis* side of the membrane with 1 mM acetate at this side. The composition of bulk solutions: 1 mM TRIS, 1 mM MES, 1 mM β-alanine, 100 mM choline chloride; pH 5.0 (curve 1), 1 mM TRIS, 10 mM MES, 10 mM β-alanine, 100 mM choline chloride; pH 5.0 (curve 2); 1 mM TRIS, 90 mM MES, 90 mM β-alanine, 100 mM choline chloride, pH 5.0 (curve 3). (*Dashed curves*) best fit curves according to Eq. 12 with parameter values: (curve 1) $A = 0.84$, $B = 0.56$, $k = 0.0039$; (curve 2) $A = 0.65$, $B = 0.90$, $k = 0.0045$; (curve 3) $A = 0.15$, $B = 0.70$, $k = 0.0030$.

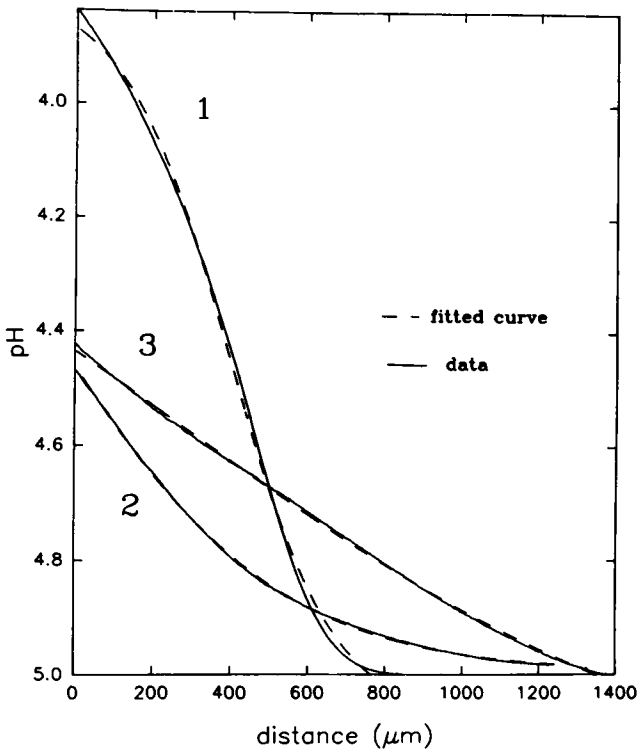

FIGURE 11 Experimental pH profiles measured at the *trans* side of the membrane with 140 mM acetate at the *cis* side. The composition of bulk solutions: 1 mM TRIS, 1 mM MES, 1 mM β-alanine, 100 mM choline chloride; pH 5.0 (curve 1), 1 mM TRIS, 10 mM MES, 10 mM β-alanine, 100 mM choline chloride; pH 5.0 (curve 2); 1 mM TRIS, 70 mM MES, 70 mM β-alanine, 100 mM choline chloride, pH 5.0 (curve 3). (*Dashed curves*) best fit curves according to Eq. 12 with parameter values: (curve 1) $A = 23.3$, $B = 18.1$, $k = 0.0074$; (curve 2) $A = 0.90$, $B = 0.69$, $k = 0.0033$; (curve 3) $A = 1.96$, $B = 1.43$, $k = 0.0014$.

the concentration profiles of permeating substances, which finally results in effects similar to "active" transport and "facilitated" diffusion across a membrane. On the other hand, proton-transfer reactions between diffusing ions may produce a thin transient layer which shows a "brake" or sharp peak of electric field (24).

In our system, the most mobile ion is H^+, and its flux is directed from the *cis* to *trans* solution. One can thus expect that the electric field in either UL has the opposite direction. If so, the action of the electric field should result in the displacement of a theoretical pH profile towards the left-hand-side solution and hence a better approximation of the experimental pH curve. This is why model 2 has been considered in this work.

Computations from model 2 showed, however, that the direction of the electric field in the ULs depends upon the bulk pH, and its magnitude is too small to alter the pH profiles significantly (Fig. 7 *A*). This is not unexpected since experiments are carried out with 100 mM of background electrolyte which decreases the diffusional potential.

(*c*) *Shifts in local chemical equilibrium.* The third possibility is that the deviations between the calculations and experimental results are due to the neglect of the finite rates of reactions 2 and 3 in model 1. Indeed, the assumption of local chemical equilibrium made in this model means that these reactions are very fast, both forward and backward. However, simple estimates show that, for example, the characteristic time of water dissociation, $\tau_W = k_{+2}^{-1} = 100$ s, exceeds the characteristic time of the hydrogen ion diffusion through the UL $\tau_D = \delta^2/D_1 = 4$ s. Besides, an important feature of the system at hand is that reactions 2 and 3 are consecutive, i.e., the H^+ ion produced by one of these reactions is utilized by the other. In this case the sufficient criterion of local equilibrium suggested earlier (25, 26) appears to be invalid. Actually, this criterion is based on the comparison of characteristic times of diffusion and of forward and backward stages of a single reaction. However, if the second reaction is much faster than the first one, it can "absorb" the product (H^+) of the first reaction, making its bimolecular stage slow and thus shifting the chemical equilibrium.

Computations with model 3 show the possibility of shift from the local chemical equilibrium of reactions 2 on an assumption that both of the reactions 3 are very fast (forward and backward). However, these shifts do not affect considerably the calculated acetate membrane flux and pH profiles.

Thus, our calculations favor model 1 as the best model for description of the permeation of acetate through the membrane in the presence of buffers. Its computational algorithm is rather simple. The use of models 2 and 3 needs much more sophisticated computations, though additional effects described by these models are not significant for our system. This discussion also shows that the most probable reason for the deviation between experimental and theoretical pH-profiles is the inconsistency of the generally accepted model of the "unstirred layer" assuming the existence of a strict boundary between the regions of "pure diffusion" and "ideal stirring".

It is worth noting that our model 1 has at least two advantages compared to the previously used models (6, 11, 12). First, it takes explicit account of buffer mixture as a source and sink for protons upon weak acid diffusion through the unstirred layer and the membrane. It is seen from Fig. 10 that the concentration of buffer controls the amplitude of pH shifts near the membrane. Second, the validity of our model is tested by comparing the experimentally measured pH profiles with theoretical predictions.

We hope that the use of model 1 (and its analogues), in spite of some of its imperfections, will enable the researchers to achieve better quantitative agreement between theoretical and experimental data on BLM transport and finally to discover better insights into the mechanisms of natural membrane functioning and action of drugs.

APPENDIX

How to solve the equations of model 1?

Let us derive a set of 5 algebraic equations linking the quantities $[\mathrm{AceH}]_L$, $[\mathrm{AceH}]_R$, $\bar{J}$, H_L and H_R. Eq. 1 is, in fact, the first of these equations.

By integrating Eqs. 8 and 4, twice with respect to x, one obtains

$$\begin{aligned} D_1c_1 - D_2c_2 - D_4c_4 - D_5c_5 - D_7c_7 &= A_{1L}x + B_{1L},\\ D_2c_2 + D_3c_3 &= A_{2L}x + B_{2L},\\ D_5c_5 + D_6c_6 &= A_{3L}x + B_{3L},\\ D_7c_7 + D_8c_8 &= A_{4L}x + B_{4L}, \end{aligned} \tag{13}$$

where A_{mL} and B_{mL} ($m = 1, \ldots, 4$) are the constants of integration.

These constants are determined using the boundary conditions (11) and (12). This yields:

$$\begin{aligned} B_{1L} &= D_1c^0_{1L} - D_2c^0_{2L} - D_4c^0_{4L} - D_5c^0_{5L} - D_7c^0_{7L};\\ B_{2L} &= D_2c^0_{2L} + D_3c^0_{3L};\quad B_{3L} = D_5c^0_{5L} + D_6c^0_{6L};\\ B_{4L} &= D_7c^0_{7L} + D_8c^0_{8L};\quad A_{1L} = A_{3L} = A_{4L} = 0;\quad A_{2L} = -\bar{J}. \end{aligned} \tag{14}$$

Now, from Eqs. 10 to 14 one obtains two additional algebraic equations linking the quantities $\bar{J}$, $H_L = c_1(\delta)$ and $[\mathrm{AceH}]_L = c_3(\delta)$:

$$D_1H_L - \frac{B_{2L} - \bar{J}\cdot\delta}{1 + H_L/K_C} - D_4\cdot\frac{K_W}{H_L} - \frac{B_{3L}}{1 + H_L/K_a} - \frac{B_{4L}}{1 + H_L/K_b} = B_{1L}; \tag{15}$$

$$[\mathrm{AceH}]_L = \frac{(B_{2L} - \bar{J}\cdot\delta)/D_2}{1 + K_C/H_L}. \tag{16}$$

By repeating the above procedure for the right-hand UL (see Fig. 1) one obtains the rest of the desired algebraic equations:

$$D_1H_R - \frac{B_{2R} + \bar{J}\cdot\delta}{1 + H_R/K_C} - D_4\cdot\frac{K_W}{H_R} - \frac{B_{3R}}{1 + H_R/K_a} - \frac{B_{4R}}{1 + H_R/K_b} = B_{1R}; \tag{17}$$

$$[\mathrm{AceH}]_R = \frac{(B_{2R} + \bar{J}\cdot\delta)/D_2}{1 + K_C/H_R}. \tag{18}$$

Here, the following designations are used:

$$B_{1R} = D_1c^0_{1R} - D_2c^0_{2R} - D_4c^0_{4R} - D_5c^0_{5R} - D_7c^0_{7R} \quad \text{and} \quad B_{2R} = D_2c^0_{2R} + D_3c^0_{3R},$$

where c^0_{iR} are the solute concentrations in the bulk of the *trans* solution.

By eliminating $[\mathrm{AceH}]_R$ and $[\mathrm{AceH}]_L$ from equations 16 and 18 and 1, we obtain the system of nonlinear equations 15, 17 and 19,

$$\bar{J} = P\cdot\left(\frac{B_{2L} - \bar{J}\cdot\delta}{1 + K_C/H_L} - \frac{B_{2R} + \bar{J}\cdot\delta}{1 + K_C/H_R}\right)\Big/ D_2, \tag{19}$$

linking the unknowns H_L, H_R and $\bar{J}$.

These equations can be solved easily, if their monotonicity is exploited. Indeed, since the left-hand side of Eqs. 15 and 17 monotonically increases with H_L and H_R for any given value of $\bar{J}$, they can be solved using the bisection method. As a result, one obtains the functions $H_L = f_L(\bar{J})$ and $H_R = f_R(\bar{J})$ (both calculated numerically). By "substituting" these functions into Eq. 19 we derive one nonlinear equation for the desired flux $\bar{J}$. Since the right-hand side of this equation monotonically decreases with increasing $\bar{J}$, it has a unique solution which can be easily computed using the bisection method.

As soon as the flux $\bar{J}$ is determined, the profiles $c_i(x)$ of solute concentrations in either UL are calculated from Eqs. 15 and 17, where H_L and H_R are substituted by $c_1(x)$ and δ is substituted by x. The solution to these equations is obtained by the same method as above.

The authors wish to thank Drs. A. A. Bulychev and L. S. Yaguzhinsky for the help with this work and fruitful discussions.

This work was partially supported by the German Academic Exchange Service.

Received for publication 23 November 1992 and in final form 16 February 1993.

REFERENCES

1. Pedley, T. J. 1983. Calculation of unstirred layer thickness in membrane transport experiments. *Quart. Rev. Biophys.* 16:115–150.
2. Barry, P. H., and J. M. Diamond. 1984. Effects of unstirred layers on membrane phenomena. *Physiol. Rev.* 64:763–972.
3. Winne, D. 1981. Unstirred layer as a diffusion barrier in vitro and in vivo In: Intestinal absorption and secretion. F. Skadhause and K. Heintse, editors. MTP-Press, Lancaster. 21–38.
4. Gutknecht, J., and D. C. Tosteson. 1973. Diffusion of weak acids across lipid bilayer membranes: effects of chemical reactions in the unstirred layers. *Science (Wash. DC).* 182:1258–1261.
5. Gutknecht, J., M. A. Bisson, and D. C. Tosteson. 1977. Diffusion of carbon dioxide through lipid bilayer membranes: effects of carbonic anhydrase, bicarbonate, and unstirred layers. *J. Gen. Physiol.* 69:779–794.
6. Walter, A., D. Hastings, and J. Gutknecht. 1982. Weak acid permeability through lipid bilayer membranes. *J. Gen. Physiol.* 79:917–933.
7. Maisterrena, B., and P. R. Coulet. 1989. Mimicked translocation of glucose and glucose 6-phosphate with artificial enzyme membranes. *Biochem. J.* 260:455–461.
8. Preston, R. L. 1982. Effect of unstirred layers on the kinetics of carrier-mediated solute transport by two systems. *Biochim. Biophys. Acta.* 688:422–428.
9. Wilson, F. A., and J. M. Dietschy. 1974. The intestinal unstirred layer: its surface area and effect on active transport kinetics. *Biochim. Biophys. Acta.* 363:112–126.
10. Winne, D. 1977. Correction of the apparent Michaelis constant, biased by an unstirred layer, if a passive transport component is present. *Biochim. Biophys. Acta.* 464:118–126.
11. Markin, V. S., V. I. Portnov, M. V. Simonova, V. S. Sokolov, and V. V. Cherny. 1987. Theory of transport of remanthadin and its analogues across membranes: intracellular pH shift, unstirred layers and membrane potentials (in Russian). *Biol. Membrany.* 4:502–523.
12. Antonenko, Y. N., and L. S. Yaguzhinsky. 1984. The role of pH gradient in the unstirred layers in the transport of weak acids and bases through bilayer lipid membranes. *Bioelectrochem. Bioenerg.* 13:85–91.
13. Antonenko, Y. N., and A. A. Bulychev. 1991a. Measurements of local pH changes near bilayer lipid membrane by means of a pH microelectrode and a protonophore-dependent membrane po-

tential. Comparison of methods. *Biochim. Biophys. Acta.* 1070:279–282.

14. Antonenko, Y. N., and A. A. Bulychev. 1991b. Effect of phloretin on the carrier-mediated electrically silent fluxes through the bilayer lipid membrane: measurements of pH shifts near the membrane by pH microelectrode. *Biochim. Biophys. Acta.* 1070:474–480.
15. Morozov, S. K., and O. P. Krasitsky. 1978. Numerical method for solving the nonstationary, spatially unidimensional, nonlinear differential equations (in Russian). *Preprint N396. IKI AN SSSR: Moscow.*
16. Walter, A., and J. Gutknecht. 1984. Monocarboxylic acid permeability through lipid bilayer membranes. *J. Membr. Biol.* 77:255–264.
17. Robinson, R. A., and R. H. Stokes. 1959. Electrolyte solutions. Academic Press, New York.
18. Bird, R. B., W. E. Stewart, and E. N. Lightfoot. 1960. Transport Phenomena. John Wiley and Sons, New York.
19. Bell, R. P. 1973. The Proton in Chemistry. Chapman and Hall, London.
20. Mueller, P., D. O. Rudin, H. Ti Tien, and W. C. Wescott. 1963. Methods for the formation of single bimolecular lipid membranes in aqueous solution. *J. Phys. Chem.* 67:534–535.
21. Yamada, H., T. Matsue, and I. Uchida. 1991. A microvoltammetric study of permeation of ferrocene derivatives through a planar bilayer lipid membrane. *Biochem. Biophys. Res. Commun.* 180:1330–1334.
22. Levich V. G. 1962. Physicochemical Hydrodynamics. Prentice-Hall, Englewood Cliffs, NJ.
23. Kozinsky, A. A., and E. N. Lightfoot. 1972. Protein ultrafiltration: a general example of boundary layer filtration. *AIChE J.* 18:1030–1040.
24. Denisov G. A., V. K. Kaluta, E. V. Nikolaev, G. A. Tishenko, L. K. Shataeva. 1992. Modeling of coupled transport of ions and zwitterions across porous ion exchange membranes. *J. Membr. Sci.* In press.
25. LeBlanc O. H. 1971. The effect of uncouplers of oxidative phosphorylation on lipid bilayer membranes: carbonilcyanide m-chlorophenylhydrazone. *J. Membr. Biol.* 4:227–251.
26. Gutknecht, J., L. J. Bruner, and D. C. Tosteson. 1972. The permeability of thin lipid membranes to bromide and bromine. *J. Gen. Physiol.* 59:486–502.